



HAL
open science

Impact of neurons on patient derived-cardiomyocytes using organ-on-a-chip and iPSC biotechnologies

Albin A Bernardin, Sarah Colombani, Antoine Rousselot, Virginie Andry,
Yannick Goumon, Côme Pasqualin, Bernard Brugg, Etienne Jacotot, Jean
Luc Pasquié, Alain Lacampagne, et al.

► **To cite this version:**

Albin A Bernardin, Sarah Colombani, Antoine Rousselot, Virginie Andry, Yannick Goumon, et al..
Impact of neurons on patient derived-cardiomyocytes using organ-on-a-chip and iPSC biotechnologies.
2022. cea-03830457

HAL Id: cea-03830457

<https://cea.hal.science/cea-03830457>

Preprint submitted on 26 Oct 2022

HAL is a multi-disciplinary open access archive for the deposit and dissemination of scientific research documents, whether they are published or not. The documents may come from teaching and research institutions in France or abroad, or from public or private research centers.

L'archive ouverte pluridisciplinaire **HAL**, est destinée au dépôt et à la diffusion de documents scientifiques de niveau recherche, publiés ou non, émanant des établissements d'enseignement et de recherche français ou étrangers, des laboratoires publics ou privés.

28 **Abstract:** In the heart, cardiac function is regulated by the autonomic nervous system (ANS)
29 that extends through the myocardium and establish junctions at the sinus node and ventricular
30 levels. Thus, an increase or decrease of neuronal activity acutely affects myocardial function
31 and chronically affects its structure through remodeling processes. The neuro-cardiac junction
32 (NCJ), which is the major structure of this system, is poorly understood and only few cell
33 models allow us to study it. Here we present an innovant neuro-cardiac organ-on-chip model
34 to study this structure to better understand the mechanisms involved in the establishment of
35 NCJ. To create such a system, we used microfluidic devices composed of two separate cells
36 compartment interconnected by asymmetric microchannels. Rat PC12 cells, were
37 differentiated to recapitulate the characteristics of sympathetic neurons, and cultivated with
38 cardiomyocytes derived from human induced pluripotent stem cells (hiPSC). We confirmed
39 the presence of specialized structure between the two cell types that allow neuromodulation
40 and observed that the neuronal stimulation impacts the excitation-contraction coupling
41 properties including the intracellular calcium handling. Finally, we also co-cultivated human
42 neurons (hiPSC-NRs) with human cardiomyocytes (hiPSC-CMs) both obtained from the same
43 hiPSC line. Hence, we have developed a neuro-cardiac compartmentalized in vitro model
44 system that allows to recapitulate structural and functional properties of neuro-cardiac
45 junction and that can be used to better understand interaction between heart and brain in
46 humans, as well as to evaluate the impact of drugs on a reconstructed human neuro-cardiac
47 system.

48 **Keywords:** organ-on-a-chip; microfluidic system; iPSC; cardiomyocytes; neurons.

49

50 **1. Introduction**

51 The cardiac function is tightly regulated by the autonomic nervous system (ANS) that extends
52 through the myocardium [1, 2]. The autonomic nervous system is composed of the
53 parasympathetic nervous system (PNS) and sympathetic nervous system (SNS) through the
54 establishment of neuro-cardiac junction (NCJ) at the sinus node and ventricular levels [1-4].
55 NCJs allow the interaction of ANS neurons and cardiomyocytes for rapid regulation of
56 homeostasis and heart integrity. The ANS also exerts a trophic action during the development
57 [5, 6] and under cardiac pathologies [4]. Thus, an increase or decrease of sympathetic activity
58 directly affects myocardial function and its structure through remodeling processes.

59 Unlike the neuromuscular junctions, synapses of the neuro-cardiac junction are poorly
60 understood. Rare studies have demonstrated the presence of protein complexes involved in
61 cellular interaction or in exocytosis [7]. The immunostaining has revealed a specialization of
62 the cardiomyocyte membrane, with a large concentration of β 1-adrenergic receptor, and a
63 decreased expression of caveolin-3.

64 The secretion of noradrenalin is involved in the development of the myocardium by the
65 tropism it exerts [8]. Dowell has demonstrated its involvement during myocardial
66 development. The specific death of sympathetic neurons by the addition of 6-
67 hydroxydopamine is directly correlated with a decrease in myocardial size [5]. Kreipke and
68 Birren showed that noradrenalin is involved in the transition between hyperplastic and
69 hypertrophic stages [6] and directly impact the size and number of cardiomyocytes (CMs).

70 Several heart conditions are associated with changes in the intracardiac neuronal network that
71 can lead to cardiac arrhythmias or an increased risk of myocardial infarction. These attacks
72 can be induced by neuronal degeneration associated with diabetes [9], sympathetic hyper-
73 innervation [10] or infection of the stellate ganglia [11] as the major sympathetic ganglion for
74 cardiac regulation [12].

75 There are very few models to study the NCJ. The cellular models are based on the use of
76 direct co-cultures in the same compartment [7, 13, 14]. Those models involve the mixing the
77 cells together in non-optimal conditions with the lack of control on specific cell population.
78 The development of microfluidic systems allows the establishment of hybrid co-culture and
79 organ-on-a-chip (OOC) with the possibility of cultivating different cell types in separate
80 compartments connected by micro-channels [15]. Spatial and fluidic compartmentalization of
81 distal axons and cell bodies replicates the in vivo conditions. Somatic and axonal milieux are

82 independently controlled. Compartmentalized devices are used in a variety of experimental
83 models ranging from isolating axons to forming neuronal networks, from creating axon co-
84 cultures to engineering axonal behavior. Such protocols have emerged in several areas of
85 research such as angiogenic development [16] or extravasation processes in tumors [17].
86 Other groups have developed similar systems to study the NCJ [13, 18, 19], demonstrating its
87 feasibility. The human induced pluripotent stem cells (hiPSC) are self-renewal and have the
88 potential to differentiate into any somatic cells. They nowadays offer great opportunities to
89 create patient-derived OOC and model key physiological and pathophysiological features of
90 human organs [20].

91 In the present study we designed an innovant neuro-cardiac OOC based on microfluidic chip
92 and hiPSC to study the impact of rat sympathetic neurons (differentiated for PC12 cells) or
93 human hiPSC-derived autonomic neurons (hiPSC-NRs) on the functional properties of
94 ventricular-like human hiPSC-derived cardiomyocytes (hiPSC-CMs).

95

96 **2. Materials and Methods**

97 *Microfluidic devices*

98 Microfluidic chips were produced by standard molding methods using epoxy-based negative
99 photoresists (SU-8) and MicroBrain Biotech proprietary microdesigns (Brainies™, Cat#:
100 MBBT5; Marly le Roi, France). Briefly, Polydimethylsiloxane (Sylgard 184, PDMS; Dow
101 Corning) was mixed with curing agent (9:1 ratio) and degassed under vacuum. The resulting
102 preparation was poured onto a chosen SU8 mold and reticulated at 70°C for 2 at least hours.
103 The elastomeric polymer print was detached, and 2 reservoirs were punched for each
104 chamber. The polymer print and a glass cover slip were cleaned with isopropanol, dried, and
105 treated for 3 minutes in an air plasma generator (98% power, 0.6 mBar, Diener Electronic)
106 and bonded together. Brainies™ MBBT5 is a chip with a design containing 4 neuronal
107 diodes. One neuronal diode includes 2 rectangular culture chambers (volume ~1 µL) each
108 connected to 2 reservoirs and separated by a series of 500 µm-long asymmetrical micro-
109 channels (3 µm high, tapering from 15 µm to 3 µm).

110 *Rat PC12 culture*

111 Rat adrenal gland (phaeochromocytoma) PC12 cells from European Collection of
112 Authenticated Cell Cultures (ECACC, 88022401) were seeded on collagen-coated 60mm petri
113 dish in complete medium. Complete medium was composed of RPMI 1640 (Gibco,

114 21875091) supplemented with 10% horse serum (Gibco, 26050088), 5% Foetal Bovine Serum
115 (Gibco, 26140079) and 12.5µg/mL gentamicin (Sigma, G1397). PC12 differentiation was
116 induced by switching from complete medium to differentiation medium. Differentiation
117 medium was composed of RPMI 1640 supplemented with 1% horse serum, 12.5µg/mL
118 gentamicin and 50ng/mL nerve growth factor (NGF, ABIN804475).

119

120 *hiPSCs maintenance and differentiation*

121 hiPSC cell lines were obtained from healthy male control. hiPSC were maintained in
122 StemFlex medium (Gibco, A3349401) on Matrigel hESC-qualified matrix (Corning, 354277)-
123 coated petri dishes at 37°C in 5% CO₂ incubator between passage 17 to 27. When the cells
124 reached confluence, cell monolayer was dissociated using Tryple express enzyme (Gibco,
125 12604013) to obtain single cell solution. We differentiated patient-specific hiPSC-derived
126 cardiomyocytes as previously published [21, 22]. hiPSC were differentiated in ventricular-like
127 cardiomyocytes using monolayer protocol and sandwich approaches [23]. The hiPSC-CMs
128 were purified using the lactate-based protocol in glucose- and pyruvate-free conditions
129 supplemented with 4mM Na-lactate as done previously [24].

130 The hiPSC-derived autonomic neurons were obtained from the same cell-line and
131 differentiated following protocols described by Montgomery group [25]. Neuronal induction
132 was launched on a cell monolayer cultured on culture dishes coated on Matrigel hESC-
133 qualified matrix. Neuronal induction was conducted for 12 days to obtain a population of
134 neurons. These neurons are seeded in microfluidic chips and matured for 42 days in co-culture
135 with hiPSC-CMs.

136

137 *Neurotransmitter release quantification*

138 The acetylcholine neurotransmitter, released in cell medium was quantified using fluorometric
139 kit (Acetylcholine, Abcam, ab65345). The four neurotransmitters were quantified in
140 supernatant of 14 days differentiated PC12 cells harvested in conditioned medium after
141 addition of Carbachol (1.5mM) in the medium.

142 Mass spectrometry was performed as follow. The cell secretion media were collected. Cells
143 were recovered in 50µl of H₂O containing 0.1mM ascorbic acid. Cells were sonicated (4 x
144 10sec, 100W; Model 505 Sonic Dismembrator; Fisher Scientific). After centrifugation

145 (20,000g, 30min, 4°C), supernatants were collected and protein concentrations were accessed
146 using the Protein Assay kit (Bio-Rad). An isotopic dilution approach was used for the
147 absolute quantification. 20µl of the cell extracts or 50µl of the secretion medium were mixed
148 with 10µl of internal standards containing 20pM of D4-Dopamine, C6-Noradrenalin, D6-
149 Adrenalin, L-DOPA in 0.1mM ascorbic acid¹. Then, 40µl of borate buffer and 10µl AccQtag
150 Ultra reagent (AccQ-Tag Ultra derivatization kit, Waters, Guyancourt, France) were added to
151 cell extracts and secretion media. The mixture was incubated 10min at 55°C under agitation.
152 500µl of ice-cold acetonitrile (ACN) were added and samples were centrifuged (20,000g,
153 30min, 4°C). The resulting supernatants were dried under vacuum and suspended in 20µl of
154 H₂O containing 0.1% formic acid (v/v).

155 Analyses were performed on a Dionex Ultimate 3000 HPLC system (Thermo Scientific)
156 coupled with an Endura triple quadrupole mass spectrometer (Thermo Electron). The system
157 was controlled by Xcalibur v. 2.0 software (Thermo Electron). 5µl of samples were loaded
158 into reverse phase Zorbax column (SB-C18, #863600-902; 1mm x 150mm, 3.5µm, Agilent
159 Technologies). Elution of the compounds was performed at a flow rate of 90 µl/min, at 40°C
160 (see supplemental table 1 for conditions). Buffer A corresponded to H₂O 98.9%/ACN
161 1%/formic acid 0.1% (v/v/v) and buffer B was ACN 99.9%/ formic acid 0.1% (v/v).
162 Dopamine, adrenalin and noradrenalin are measured using the multiple reaction monitoring
163 mode (MRM) according to the settings. The targeted compounds are detailed in supplement
164 tables 2 and 3. The selection of the monitored transitions and the optimization of the collision
165 energy (CE) were manually determined. The identification of the compounds was based on
166 precursor ions, daughter ions and retention times obtained for dopamine, adrenalin and
167 noradrenalin and their corresponding internal standards. Amounts of neurotransmitters were
168 quantified according to the isotopic dilution method [26].

169

170 *PC12/hiPSC-CMs co-culture*

171 The day before neuronal seeding, chips were UV-sterilized for 20 min, then coated with a
172 solution of poly-D-lysine (10 µg/ml, Sigma, P6407), incubated overnight (37°C, 5% CO₂),
173 and rinsed 3 times with Dulbecco's phosphate buffer saline (PBS) (Sigma, D8537). Then, 4
174 hours before cell seeding, chips were treated with a solution of Laminin (10 µg/mL: Sigma) in
175 PBS. Undifferentiated PC12 cells were seeded in microfluidic devices in differentiation
176 medium supplemented with 50ng/mL of NGF and differentiated for 5 days. During this phase,
177 PC12 started to differentiate with the formation of neurites and started projecting into micro-

178 channels and invaded cardiac compartment. At day 5, hiPSC-CMs aged between 11 days and
179 20 days were seeded on Matrigel hESC-qualified matrix with a density of 20 000
180 cells/compartment in B27 medium supplemented with 10 μ M Rock inhibitor and NGF at
181 150ng/ml. Complete medium changes with corresponding NGF concentrations were
182 performed once a week to avoid cell detachment.

183 For neuro-cardiac OOC between hiPSC-NRs and hiPSC-CMs, autonomic neurons are seeded
184 in neuronal compartment on Matrigel hESC-qualified and matured for 7 days before
185 cardiomyocytes seeding without addition of NGF. Once the cardiomyocytes seeded, co-
186 culture started for 30 days to allow neurites to invade cardiac compartment and create
187 interaction with CMs.

188

189 *Immunocytochemistry*

190 Immunocytochemistry (ICC) were performed 14 days after cells seeding on chips. Classical
191 ICC protocols have been adapted to microfluidic chips to avoid liquid flux and cell
192 detachment. Cells in neuronal and cardiac compartments were fixed with 4% PFA for 15
193 minutes at room temperature then rinsed 3 times with PBS. Cell membranes were
194 permeabilized with 0.1% Triton for neuronal cells and 0.01% Triton for cardiac cells in PBS,
195 10min at room temperature followed by blockade solution (1% BSA in PBS) for 30min at
196 room temperature. Primary antibodies were diluted in PBS supplemented with 0.1% BSA and
197 incubated at 4°C overnight and rinse three times with PBS. Secondary antibodies were diluted
198 in PBS and 0.1% BSA and incubated 2 hours at room temperature supplemented with 40,6-
199 diamidino-2-phenylindole (DAPI, 1:2000). Antibodies are listed in supplemental table 4. The
200 chips were stored hydrated at 4°C before use. Staining was obtained with inverted microscope
201 Axio Observer Z1 coupled with laser scanning confocal microscope LSM800 piloted with
202 Zen 2.5 software, all provided by Zeiss. ICC images were acquired in 3D with z-stack option
203 and reconstructed with ImageJ.

204

205 *Intracellular calcium dynamics*

206 Intracellular calcium signaling was studied to confirm the modulation of cardiac functional
207 properties after neuronal stimulation. Calcium transient (CaT) were recorded with cytosolic
208 free calcium probe Fluo-4 AM (Molecular Probes™, F14201) as published before [27, 28].
209 Cells were incubated with 1 μ M probe for 15 minutes at 37°C in Tyrode solution (in mM: 135

210 NaCl, 4 KCl, 1.8 CaCl₂, 1 MgCl₂, 10 HEPES, 10 glucose, 0.1 acid ascorbic, pH 7.4).
211 Calcium transients were recorded for 7 seconds in line-scan mode using LSM800 confocal
212 microscope (Zeiss) and analyzed using PeakInspector as done before [21, 22, 29].

213

214 *Measurement of contractile function using video-edge capture*

215 To assess the contractile properties of the hiPSC-CMs connected with the neurons, we
216 perform the video-edge capture as done before [21, 22] on microfluidic chip after 14 days of
217 co-culture. Activity of connected cardiomyocytes were recorded for 25 seconds. Transmitted
218 light video at 63frame/s (fps) were obtained with LSM800 confocal microscope (Zeiss) at x63
219 magnification with ORCA-Flash4 camera (Hamamatsu). Experiments were performed in
220 Tyrode solution (in mM: 135 NaCl, 4 KCl, 1.8 CaCl₂, 1 MgCl₂, 10 HEPES, 10 glucose, 0.1
221 acid ascorbic, pH 7.4). The movement of each pixel in the image was evaluated using a
222 patented video analysis script (Autobeats) via MATLAB software [21, 22]. This analysis
223 provides a contraction versus time curve from which contractile properties are extracted.

224

225 *Statistical analysis*

226 All data are expressed as the mean±SEM. Statistical analysis was performed with GraphPad
227 Prism 8.0.1 (GraphPad Software Inc.). Experimental groups were compared by using non-
228 parametric Kruskal-Wallis tested followed by Dunn's multiple comparisons test were
229 performed. P<0.05 was considered statistically significant.

230

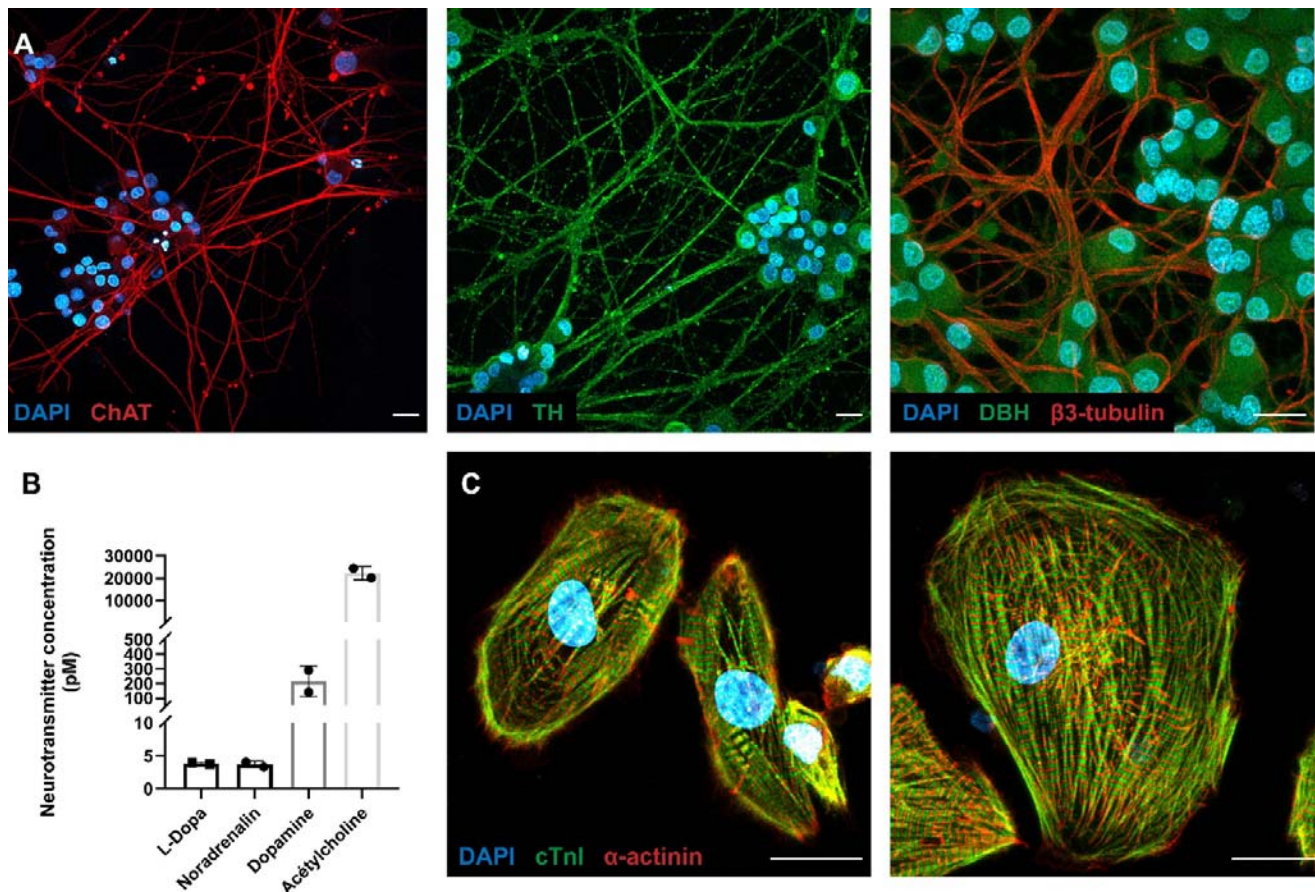
231 **3. Results**

232 *3.1. Molecular characterization of the PC12 neurons connected with hiPSC-CMs*

233 Rat PC12 cells were differentiated for 14 days in classic petri dish. Neurotransmitter
234 production was confirmed by ICC showing the expression of enzymes involved in
235 neurotransmitter production: choline acetyltransferase (ChAT) for acetylcholine, tyrosine
236 hydroxylase for all the catecholamines (TH) and dopamine β-hydroxylase (DBH) for
237 noradrenalin. ICC showed that PC12 expressed both TH and ChAT in neurites and DBH in
238 their soma (Figure 1A), suggesting a production of these neurotransmitters. Despite these
239 staining, we were unable to measure catecholamines with ELISA kits (Abnova, KA3836)
240 compared to acetylcholine, which could be measured with fluorometric kits (Abcam,

241 ab65345). The neurotransmitter quantification was performed in cell supernatant after
242 addition of 1.5mM Carbachol. Medium was collected 2min after neuronal stimulation. Our
243 results showed a larger secretion of acetylcholine ($24.39 \cdot 10^3$ pM) than catecholamines or their
244 precursors (noradrenalin: 3.7 pM, L-DOPA: 3.8 pM, dopamine: 214.6 pM) in PC12 (Figure
245 1B), suggesting a dominant parasympathetic profile of these neurons.

246 As published before [21, 22, 30] we confirmed that we generated ventricular-like hiPSC-CMs
247 through the expression of the sarcomeric cardiac markers including α -actinin and cardiac
248 troponin I (cTnI) at 30-days of differentiation (Figure 1C).



249

250 **Figure 1.** Molecular characterization of neuro-cardiac OOC composed of PC12 cells and hiPSC-CMs. (A)
251 PC12 cells differentiate into parasympathetic neurons. PC12 were cultured for 14 days in the presence of
252 50ng/ml NGF, fixed and immunolabelled for sympathetic markers. Representative immunofluorescence
253 microscopy images show choline acetyltransferase (left panel; in red), tyrosine hydroxylase (central panel; in
254 green), dopamine β -hydroxylase (Right panel; in green), and β 3-tubulin (Right panel; in red). (B) Quantification
255 of neurotransmitters in supernatant of PC12 cells. PC12 cells were differentiated for 14 days and subjected to
256 addition of 1.5mM Carbachol for 2 min. Then, medium was collected and the indicated neurotransmitters were

257 *quantified as described in material and method section. (C) hiPSCs differentiate in cardiomyocytes (hiPSC-*
258 *CMs) after 30 days following the so-called “matrix sandwich method” of differentiation. hiPSC-CMs were fixed*
259 *and immunolabelled for sarcomeric cardiac markers. Representative immunofluorescence microscopy images*
260 *show Cardiac troponin (in green) and the α -sarcomeric actinin (in red). Scale bars: 20 μ m.*

261

262 *3.2. Microfluidic devices allow a neuro-cardiac OOC.*

263 Twenty year ago, Taylor et al., used a microfabricated silicon wafer to mold a silicone
264 elastomer (namely polydimethylsiloxane) that featured two chambers connected by parallel
265 microgrooves. Once sealed against a glass coverslip microgroove formed microchannels [31,
266 32]. The resulting devices were developed in many ways by multiples research groups to
267 compartmentalize and study neurons as well as neuronal networks in various physiological
268 and pathological contexts [33].

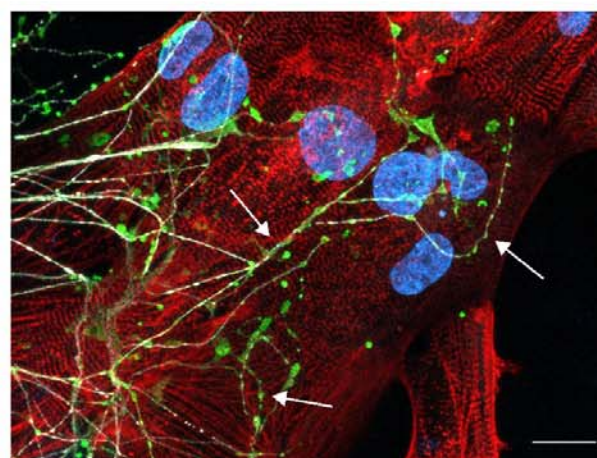
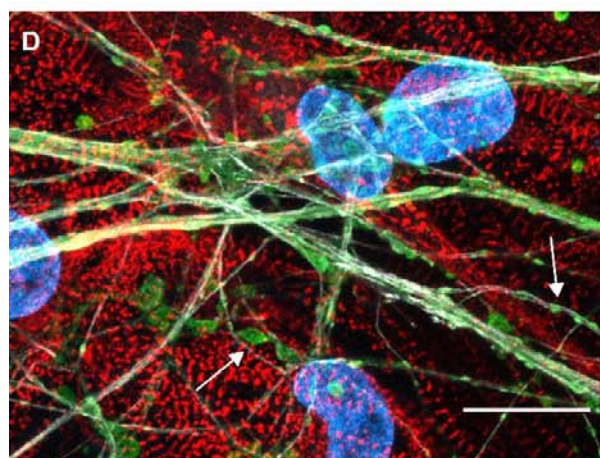
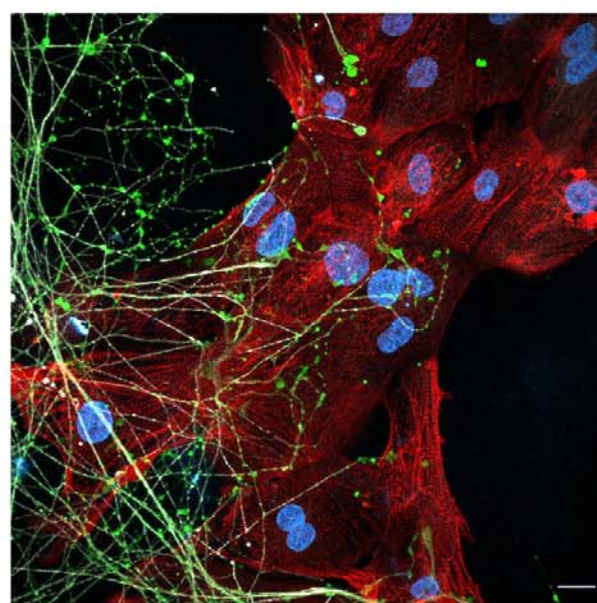
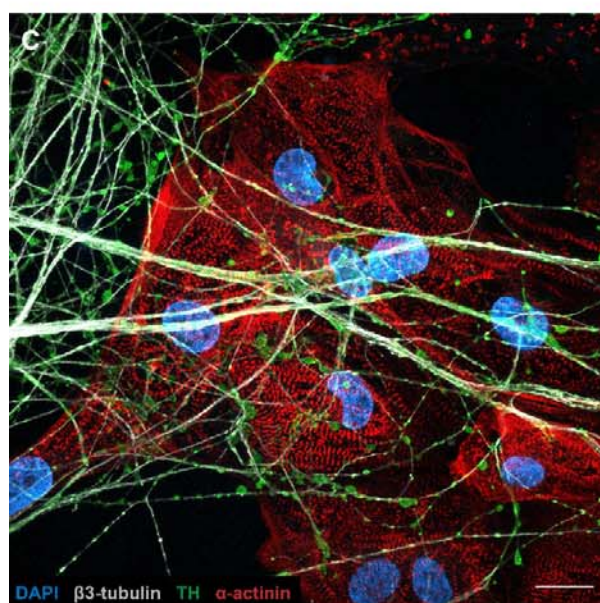
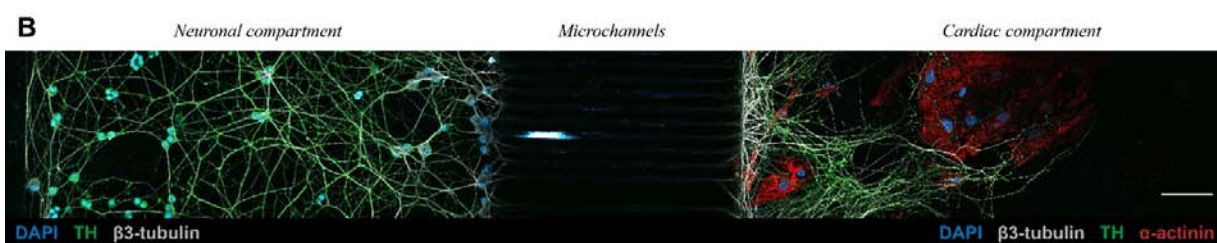
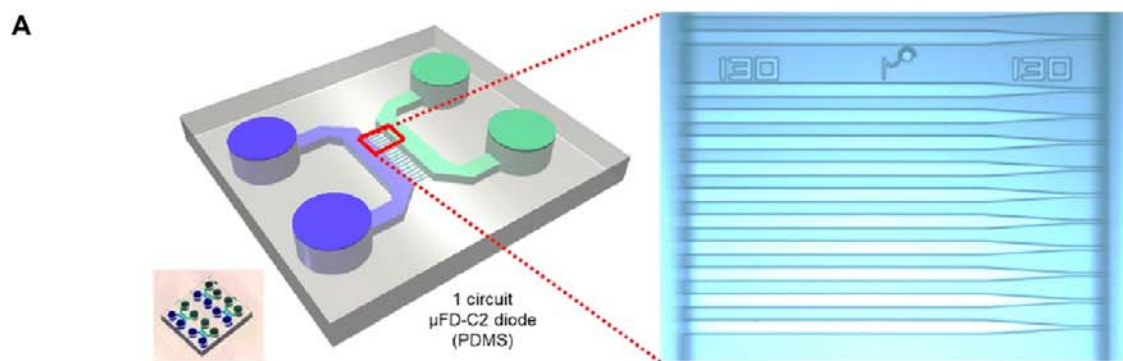
269 Neuronal diodes are fluidic microsystems, inspired by those of Taylor et al., conceived to
270 impose directionality when connecting two neuronal populations [34]. Neuronal diodes are
271 made up of two separate cellular micro-compartments interconnected by a series of
272 asymmetric microchannels, each of whose openings were of different sizes (Figure 2A). Here
273 we have used a slightly modified and standardized design of the two-chamber neuronal diode
274 (Figure 1; Brainies® MBBT5) and seeded neurons in the compartment where the
275 microchannels openings were widest (15 μ m) and cardiomyocytes in the second compartment,
276 where the openings were very narrow (3 μ m). The expectation of such cocultures is to
277 separate the (somato-dendritic) neuronal compartment from the cardiomyocytes compartment,
278 and to obtain axonal projections through the microchannel to analyze axon-dependent neuron
279 to cardiomyocytes interactions. The characteristics of the device combined with the controlled
280 filling of each reservoirs allow fluidic isolation between chamber and the so-called
281 compartmentalized pharmacology where treatment can be added selectively in one chamber
282 but not the opposite.

283

284 *3.3. PC12/hiPSC-CMs OOC involves neuro-cardiac junctions and synapse-like* 285 *junctions*

286 Undifferentiated PC12 cells were seeded in neuronal compartment with 50ng/mL of NGF.
287 Cells started differentiating in neuron-like cells through neurites from the soma. NGF gradient
288 concentration was created between neuronal (50ng/ml) and cardiac compartment (150ng/ml)

289 to attract neurites. At day 5 post PC12 seeding, we observed neurites projecting into
290 microchannel and started invading the cardiac compartment (Figure 2B). hiPSC-CMs were
291 seeded at this day and OOC are co-cultured for 14 days. This procedure allowed us to obtain
292 reproducible and transposable co-cultures protocols. During the 14 days of co-culture, PC12
293 neurites continued to develop in cardiac compartment and projected in every direction to
294 make numerous interactions with cardiomyocytes (Figure 2C). At the end of microchannels,
295 PC12 projections were organized in network of large neurites. This network divided in several
296 smaller neurites systems that projected in all directions and interacted with the hiPSC-CMs.

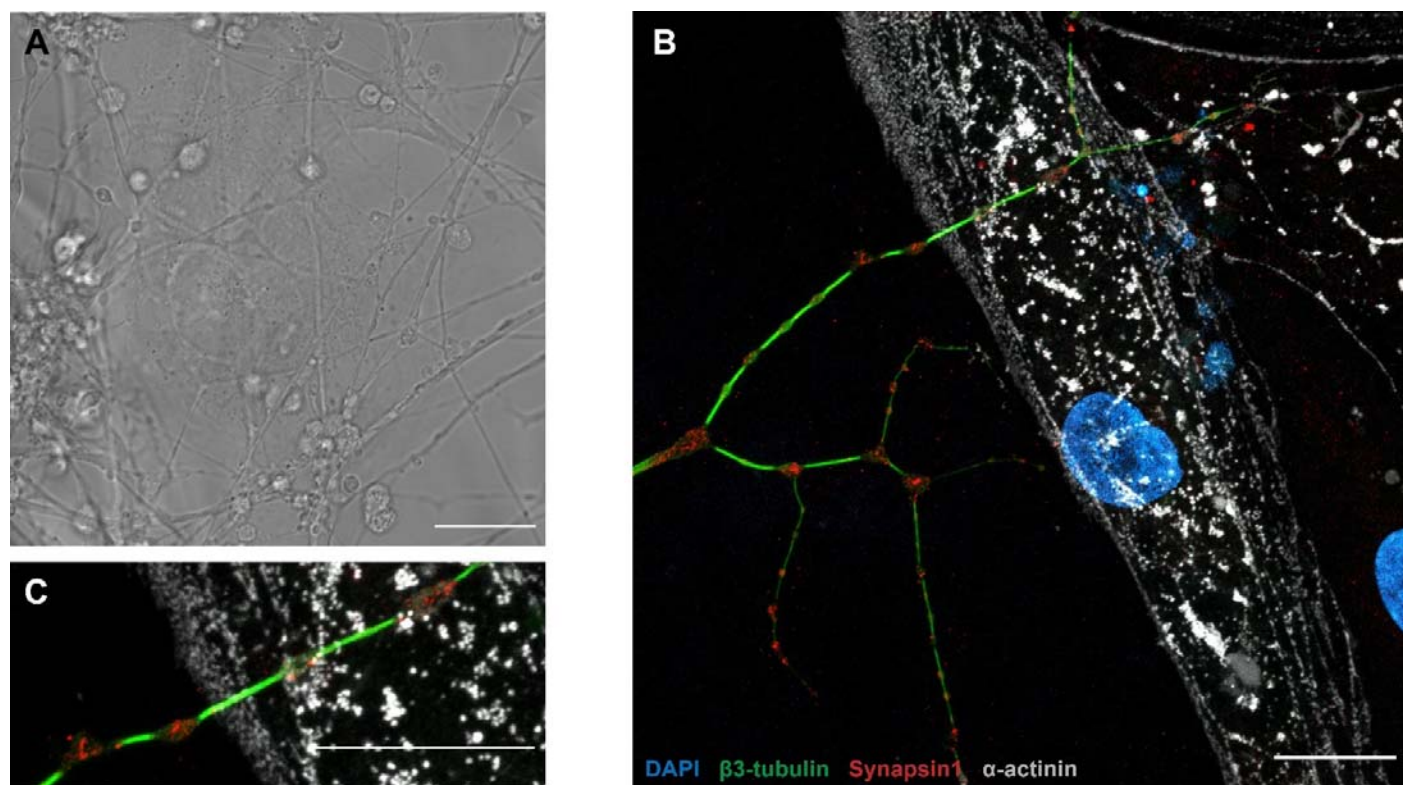


298 **Figure 2.** *Neuronal diodes fluidic microsystems as a tool to establish compartmentalized neurocardiac co-*
299 *culture on chip. (A) Structural characteristics of a two-chamber neuronal diode also known as Brainies®. Left*
300 *panel: 3D-model of the micro-structured PDMS-based block (grey), including cy-lindric wells (diameter: 4 mm;*
301 *height: 5 mm), rectangular cell culture chambers (vol. ~1 μ L; height: 55 μ m), and series of asymmetrical*
302 *microchannels (length: 500 μ m; height: 3 μ m; width: tapering from 15 μ m to 3 μ m). The compartment where*
303 *neurons are seeded is represented in blue and the compartment where cardiomyocytes are seeded is represented*
304 *in green. Small in-sert shows a picture of one Brainies® that contains four neuronal diodes. Right panel: micro-*
305 *graph of a portion of the funnel-shaped microchannels. (B) In this fluorescence microscopy image of a*
306 *microfluidic chip section, the neural compartment is located to the left and the cardiac compartment to the right.*
307 *Between the two compartments are the microchannels (not visible in the image, scale bar: 100 μ m). PC12 cells*
308 *differentiate directly into their compartments and their axons project into the cardiac compartment through the*
309 *channels. (C) and (D): Images of neuro-cardiac interactions in cardiac compartments after 14 days of co-*
310 *culture. Tyrosine hydroxylase (in Green) appear apposed along axons. Axons (β 3-tubulin; in white) harbor*
311 *varicosities in the interaction zones (White arrows). (Blue: DAPI, Red: sarcomeric α -actinin, Green: Tyrosine*
312 *hydroxylase, White: β 3-tubulin, scale bar: 20 μ m).*

313

314 Previous studies have shown that the neurocardiac junction is a specialized structure that
315 exhibits a specific cellular organization of neuronal and cardiac cells [7, 14]. *In vivo*,
316 sympathetic neurons project along cardiac tissue and form buds with cardiomyocytes. This
317 morphology is referred as the pearl necklace structure [35]. These axonal sprouting are also
318 called varicosity, which contain the cardiac synapse releasing the neurotransmitter. Due to
319 their secretory activity and interaction with cardiomyocytes, varicosities express a panel of
320 proteins involved in the release of neurotransmitters like synapsin-1 [7] or proteins involved
321 in intercellular interaction like SNARE proteins [36].

322 To confirm the presence of synapses between PC12 neurites and hiPSC-CMs, we performed
323 immunofluorescence experiments and acquired images in transmission light. Our results
324 revealed that PC12 neurites interacted densely with hiPSC-CMs and form varicosity-like
325 structures (Figures 2D and 3A). To confirm the presence of synapses, we revealed expression
326 of synapsin-1 and β 3-tubulin following 14 days of co-culture using fluorescence microscopy.
327 Our immuno-staining showed that neurites reproduced pearl necklace organization close to
328 the hiPSC-CMs with the specific expression of synapsin-1 localized in the buds (Figure 3B).



329

330 **Figure 3.** Structural characterization of the neuro-cardiac junction on a 14-day-old OOC. Images showing
331 regions of local interaction between PC12 axons and hiPSC-CM in transmission light (A) or in
332 immunofluorescence (B). PC12 neurites express the protein synapsin-1 colocalized with structural staining (β -
333 tubulin; green) in regions of interaction with cardiomyocytes and neurites. (C): Co-localization of tyrosine
334 hydroxylase and synapsin-1 in the varicosities outside the neurocardiac junctions. (In this figure: blue: DAPI,
335 red: synapsin-1, Green: β 3-tubulin, Grey: sarcomeric α -actinin, scale bar: 20 μ m).

336

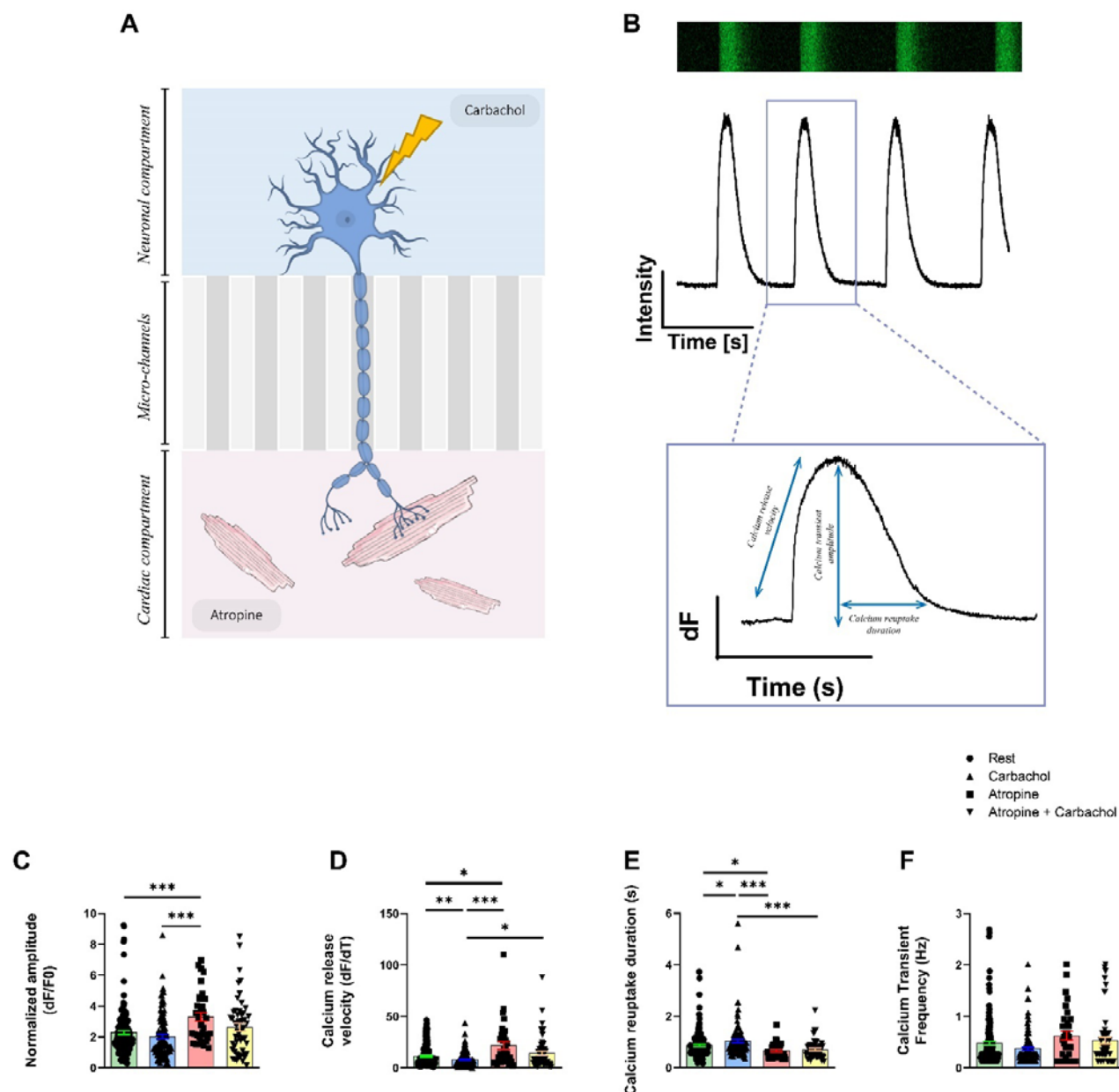
337 3.4. Neurons modulate the intracellular calcium handling in hiPSC-CMs

338 We then hypothesized that PC12 neuronal cells could modulate the ECC of the hiPSC-CMs
339 via NCJ. We focused on the intracellular Ca^{2+} handling and contractile properties as two
340 major aspects of the ECC. We designed a protocol to apply drugs independently in the
341 neuronal and cardiac compartments (Figure 4A). Using Fluo4-AM and fluorescent
342 microscopy, we acquired CaT at rest and in presence of Carbachol (muscarinic receptor
343 agonist) in the neuronal compartment or Atropine (muscarinic receptor antagonist) in the
344 cardiac compartment (Figure 4B). Their effects were studied just after addition of drugs in the
345 corresponding compartments. We focused on the relative CaT amplitude as indicator of the

346 sarcoplasmic reticulum (SR) Ca^{2+} content, velocity of Ca^{2+} release through type 2 ryanodine
347 receptor (RyR2), Ca^{2+} reuptake duration and CaT frequency (Figure 4C).

348 Release of neurotransmitter after stimulation of PC12 cells by carbachol in neuronal
349 compartment affects the Ca^{2+} kinetics in cardiomyocytes (Figure 4D-F). The CaT frequency
350 (Rest: 0.48 ± 0.04 Hz, Carbachol: 0.38 ± 0.03 Hz, Atropine: 0.63 ± 0.09 Hz, Atropine + Carbachol:
351 0.53 ± 0.07 Hz, $p = \text{ns}$) was not affected by the different experimental conditions in
352 cardiomyocytes (Figure 4F). Addition of carbachol did not modulates the CaT amplitude
353 (Rest: 2.28 ± 0.13 , Carbachol: 2.03 ± 0.14 , $p = \text{ns}$, Figure 4C) but affected Ca^{2+} release velocity
354 after PC12 stimulation (Rest: 11.41 ± 0.86 , Carbachol: 7.76 ± 0.73 , $p < 0.01$, Figure 4D) and Ca^{2+}
355 reuptake duration (Rest: 0.87 ± 0.04 s, Carbachol: 1.04 ± 0.07 s, $p < 0.05$, Figure 4E).

356 Blockade of M2 muscarinic receptor by the application of atropine in the cardiac
357 compartment induced an increase of Ca^{2+} release velocity in hiPSC-CMs compared to rest
358 condition (Rest: 11.41 ± 0.86 , Atropine: 21.54 ± 3.72 , $p < 0.05$), after addition of carbachol
359 (Carbachol: 7.76 ± 0.73 , Atropine: 21.54 ± 3.72 , $p < 0.001$) and after addition of both molecules
360 combined (Atropine: 21.54 ± 3.71 , Atropine + Carbachol: 14.14 ± 2.10 , $p < 0.05$) (Figure 4D).
361 Addition of atropine also induced a decrease of Ca^{2+} reuptake duration compared to rest (Rest:
362 0.87 ± 0.04 s, Atropine: 0.66 ± 0.05 s, $p < 0.05$) or to carbachol-treated PC12 cells (Carbachol:
363 1.04 ± 0.07 s, Atropine: 0.660 ± 0.047 seconds, $p < 0.001$) or both combined (Carbachol:
364 1.042 ± 0.068 seconds, Atropine + Carbachol: 0.71 ± 0.05 s, $p < 0.001$) (Figure 4E). Finally, we
365 also observed that addition of atropine significantly increased Ca^{2+} transient amplitude
366 compared to rest (Rest: 2.28 ± 0.13 , Atropine: 3.30 ± 0.28 , $p < 0.001$) and to carbachol condition
367 (Carbachol: 2.09 ± 0.17 , Atropine: 3.30 ± 0.28 , $p < 0.001$) (Figure 4C).



368

369 **Figure 4.** Monitoring of the intracellular calcium cycling properties on 14-day-old neuro-cardiac OOC using
 370 PC12 and hiPSC-CMs. (A) Schematic representation of neurocardiac OOCs with cellular compartments
 371 showing where the different molecules are added. The M2 muscarinic receptor antagonist atropine is added to
 372 the cardiac compartment and the muscarinic receptor agonist Carbachol is added to the neuronal compartment.
 373 (B) CaT are recorded using Fluo4-AM. Representation of CaT in hiPSC-CMs recorded in line-scan
 374 configuration with the corresponding plot below from which calcium kinetics are obtained. (C) Parameters of
 375 normalized amplitude of CaT, (D) calcium release velocity, (E) duration of Ca^{2+} reuptake and (F) frequency of
 376 CaT are presented in resting condition, after addition of carbachol and or atropine on the cardiomyocytes
 377 located in the cardiac compartment after 14 days of co-culture. Data are presented as mean \pm SEM, Rest n=145,

378 *Carbachol* $n=108$, *Atropine* $n=34$, *Carbachol + Atropine* $n=55$. Dunn's multiple comparisons test were
379 performed, * $p<0.05$, ** $p<0.01$, *** $p<0.001$.

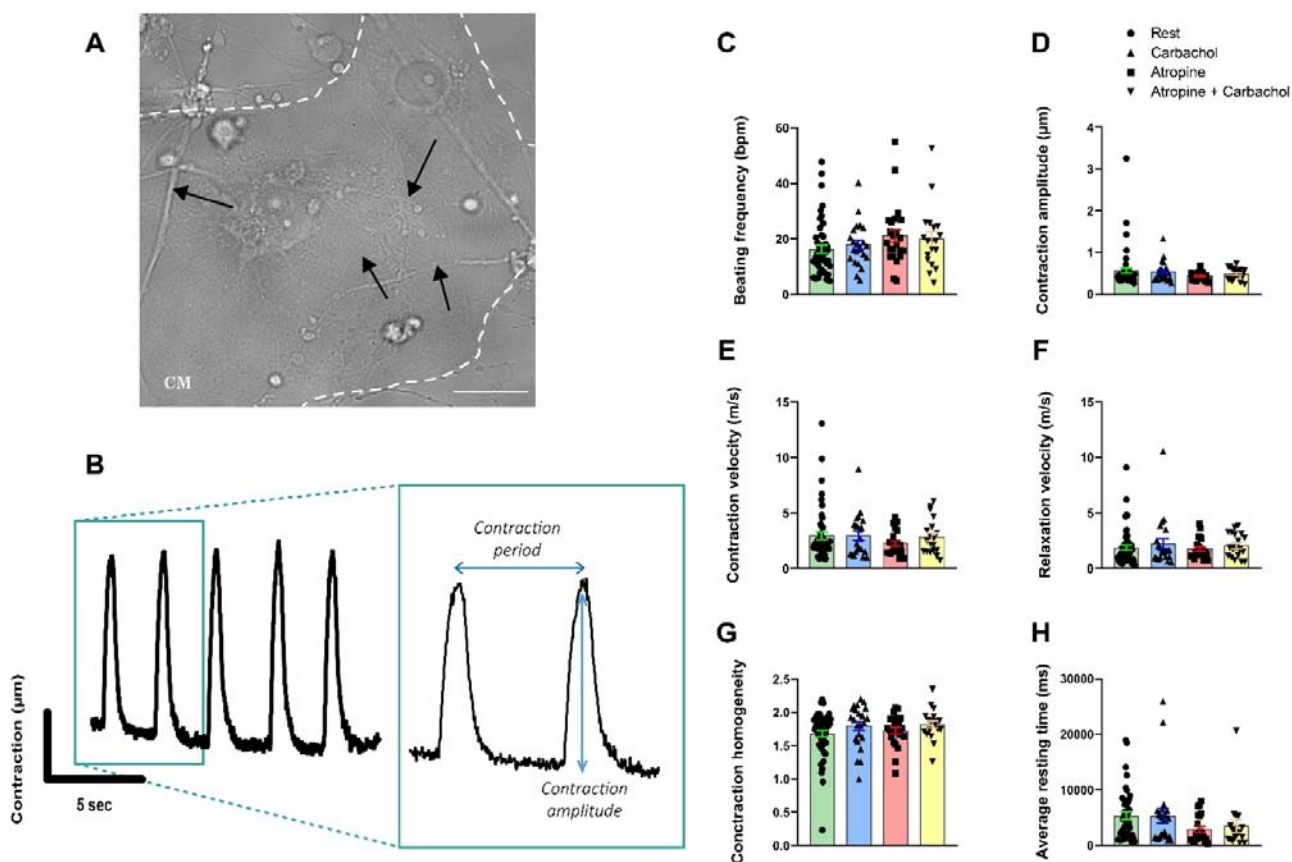
380

381 *3.5. Neurons do not impact the contractile properties in hiPSC-CMs*

382 We next evaluated whether neurons could modulate the contractile properties of the hiPSC-
383 CMs using the video-edge capture, as published before [21, 22], in microfluidic chips in
384 transmitted light at rest (Figure 5A) and in the presence of Carbachol and/or Atropine. The
385 contractility was first measured at rest for 25s, then after addition of Carbachol or Atropine.
386 An example of the obtained contraction/relaxation cycle is shown in Figure 5B.

387 Acetylcholine release from PC12 neurites following the addition of Carbachol has no effects
388 on contraction parameters (Figure 5 C-H). The contraction frequency in beats/min (Rest:
389 16.28 ± 1.39 bpm, Carbachol: 17.85 ± 1.63 bpm, $p=ns$, Figure 5C), contractile amplitude (Rest:
390 0.57 ± 0.07 , Carbachol: 0.54 ± 0.05 , $p=ns$, Figure 5D), contraction velocity (Rest:
391 2.94 ± 0.34 m/s, Carbachol: 2.94 ± 0.39 m/s, $p=ns$, Figure 5E), relaxation velocity (Rest:
392 1.87 ± 0.24 m/s, Carbachol: 2.23 ± 0.44 m/s, $p=ns$, Figure 5F), contraction homogeneity (Rest:
393 1.68 ± 0.05 , Carbachol: 1.79 ± 0.07 , $p=ns$, Figure 5G) and the resting time (Rest:
394 5310 ± 663.6 ms, Carbachol: 5304 ± 1318 ms, $p=ns$, Figure 5H). Surprisingly, addition of
395 Atropine had no effects on the contractile properties compared to the results obtained with
396 calcium experiments (Figure 4C-F) suggesting that spontaneous acetylcholine release is not
397 sufficient to modulate the contraction frequency (Rest: 16.28 ± 1.39 bpm, Atropine: $21.15\pm$
398 2.34 bpm, Atropine + Carbachol: 20.05 ± 2.57 bpm, $p=ns$, Figure 5C), the amplitude of
399 contraction (Rest: 0.57 ± 0.07 , Atropine: 0.44 ± 0.02 , Atropine + Carbachol: 0.48 ± 0.03 , $p=ns$,
400 Figure 5D), the contraction velocity (Rest: 2.94 ± 0.34 m/s, Atropine: 2.28 ± 0.22 m/s, Atropine +
401 Carbachol: 2.85 ± 0.37 m/s, $p=ns$, Figure 5E), the relaxation velocity (Rest: 1.87 ± 0.24 m/s,
402 Atropine: 1.79 ± 0.18 m/s, Atropine + Carbachol: 2.08 ± 0.25 m/s, $p=ns$, Figure 5F), the
403 contraction homogeneity (Rest: 1.68 ± 0.05 , Atropine: 1.73 ± 0.05 , Atropine + Carbachol:
404 1.82 ± 0.05 , $p=ns$, Figure 5G) and resting time (Rest: 5310 ± 663.6 ms, Atropine: $2880 \pm$
405 518.9 ms, Atropine + Carbachol: 3433 ± 1082 ms, $p=ns$, Figure 5H).

406



407

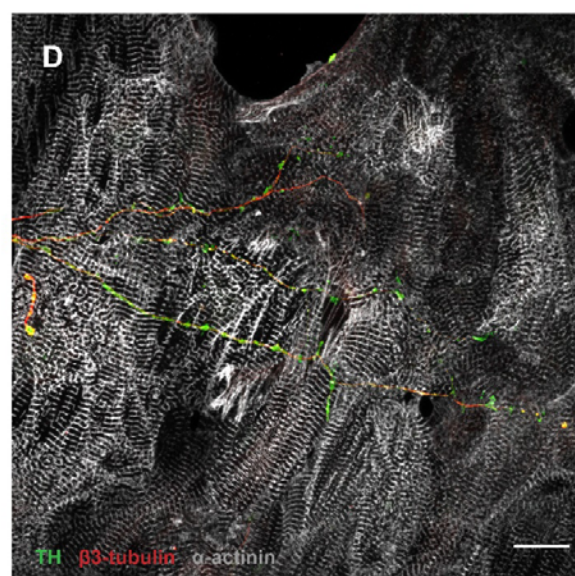
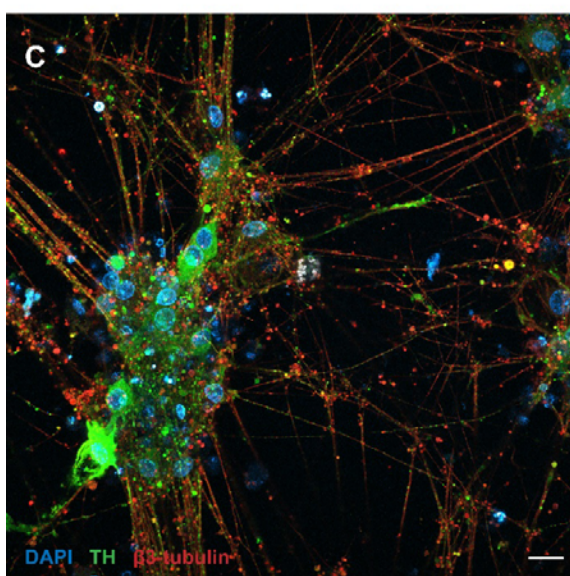
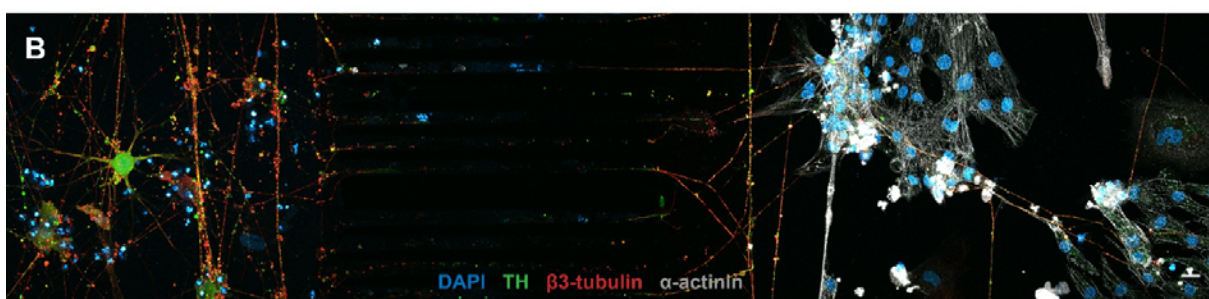
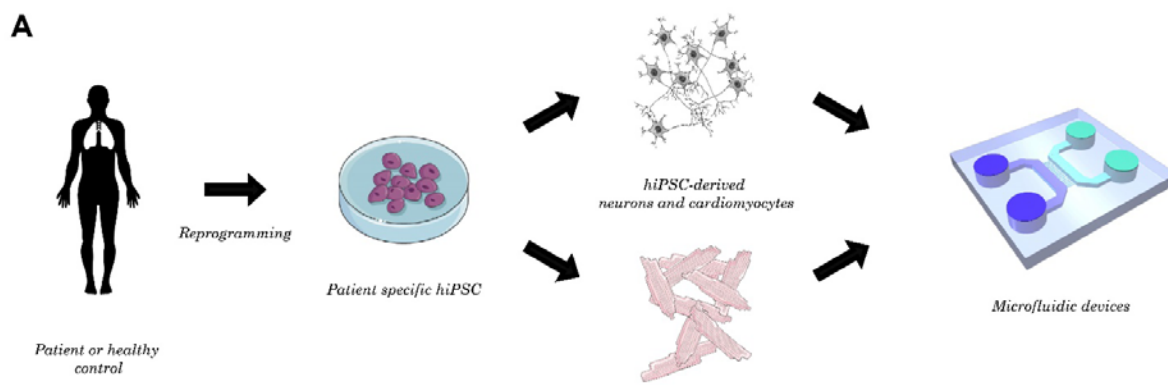
408 **Figure 5.** Contractile properties of hiPSC-CMs recorded in 14-day-old neuro-cardiac OOC by video-edge
 409 capture. (A) Picture of PC12 neurites connected (marked with black arrows) to hiPSC-CMs in transmitted light.
 410 Spontaneous contraction is recorded on cardiac compartment for 25 seconds. (B) Representation of
 411 contraction/relaxation cycle obtained from movies. (C-H) Measurement of contractile parameters on neuro-
 412 cardiac OOC at rest, in the presence of Carbachol, Atropine, or in the presence of both. (C) Beating frequency,
 413 (D) amplitude of contraction, (E) contraction and (F) relaxation velocity, (G) contraction homogeneity and (H)
 414 average resting time are obtained from series of images as shown in Figure 5A. Data are presented as mean \pm
 415 SEM, Rest $n=49$, Carbachol $n=23$, Atropine $n=23$, Carbachol + Atropine $n=19$, Dunn's multiple comparisons
 416 test were performed.

417

418 3.6. Patient-specific neuro-cardiac OOC using hiPSC-NRs and hiPSC-CMs

419 In order to confirm the feasibility of such neuro-cardiac OOC using the same hiPSC line to
 420 generate neurons and cardiomyocytes, we differentiated TH-positive hiPSC-NRs that we co-
 421 cultivated with hiPSC-CMs in microfluidic devices (Figure 6A). The hiPSC-NRs were seeded
 422 in microfluidic compartment at the beginning of neuronal maturation 1 week before
 423 cardiomyocytes seeding. They were able to create numerous interactions with the projection

424 of other neurons (Figure 6C) and to project into microchannels to invade cardiac compartment
425 without NGF addition (Figure 6B). These neurons generated numerous interactions with one
426 or several cardiomyocytes after 14 days of co-culture (Figure 6D).



427

428

429

430 **Figure 6.** *Neuro-cardiac OOC using neurons and cardiomyocytes derived from the same patient-derived*
431 *hiPSC line. (A) Schematic presentation of the production of patient-specific neuro-cardiac OOC using similar*
432 *control hiPSC line to generate autonomic neurons and cardiomyocytes. (B) Global view of neuro-cardiac*
433 *interaction after 14 days in microfluidic chips of autonomic hiPSC-NRs seeded in neuronal compartment (C)*
434 *projecting to the cardiac compartment. (D) Autonomic neurons expressing TH create projection that cross the*
435 *microchannels and interact with cardiomyocyte (Blue: DAPI, Red: sarcomeric α -actinin, White: β 3-tubulin,*
436 *Green: TH, scale bar: 20 μ m).*

437

438 **4. Discussion**

439 In this study, we built-up a neuro-cardiac OOC to investigate the functional impact of neurons
440 on patient-derived cardiomyocytes. OOC approaches emerge with different protocols in order
441 to study the effect of interaction between cardiac and neurons with the use of direct co-culture
442 [13, 14, 37, 38] or microfluidic devices. Compared to direct co-culture, microfluidic chips
443 allow the culture of each cell-lines in their optimal conditions. Fluidic isolation of each
444 chamber also allows to ensure cell-type specific pharmacological treatments. Here, our results
445 indicate that neurons seeded in one compartment are able to further differentiate and spread
446 axons into microchannels to reach the cardiac compartment containing hiPSC-CMs. The
447 width and length of microchannels only allows axon to reach the second compartment,
448 whereas neither dendrites and soma, nor cardiomyocytes can access the opposite
449 compartment.

450 Our data show that axons form a large network at the end of microchannels. Via a large
451 spread, they subdivide in thin filaments which spread in all the directions to create interaction
452 with hiPSC-CMs. This axonal network is the central element of neurocardiac regulation [39].
453 In physiological conditions, it has been shown that neurites spread on long distances from one
454 cardiomyocyte to another and interact with them by forming buddings along axons. These “*en*
455 *passant*” structures, also called varicosities, are the functional neurotransmitter release site
456 that enables rapid and axial neurotransmitter release to several cardiomyocytes at the same
457 time [39]. As published by other groups, these varicosities are a specialized and ordered
458 structure on either sides of the synaptic cleft that induces rapid activation of β -adrenergic
459 signaling pathway [14]. In neuromuscular junction, these structures are also observed with
460 high concentration of nicotinic receptors at the post-synaptic side [40].

461 To confirm development of functional synapse between PC12 cells and hiPSC-CMs, we
462 performed structural and functional characterization of the neuro-cardiac junction. The NCJ
463 and its proteins are not very well known. In our study, we focused on the presence of
464 varicosities in neuronal network. We confirmed that expression of synapsin-1, a key synapse
465 protein, at the neuro-cardiac interaction zone. Synapsin-1 is a protein expressed in neuronal
466 synapse to organize vesicles pools, maturation and neurotransmitter release [36, 41, 42]. In
467 our neuro-cardiac OOC, we found that some structures similar to varicosities co-localized
468 with synapsin-1. These observations strongly suggest that PC12 axons and cardiomyocytes
469 form a NCJ-like structure and synapses *in vitro*. Further experiments using electronic
470 microscopy could confirm such specialized structure by showing organized cell membrane in
471 neurons and cardiomyocytes.

472 Our findings revealed that PC12 cells express both adrenergic (DBH and TH) and cholinergic
473 (ChAT) enzymes but secrete a larger amount of acetylcholine compared to catecholamine
474 resulting rather in a parasympathetic than sympathetic neurotransmitters pattern. This
475 observed phenotype makes sense with our results on the intracellular Ca^{2+} handling properties
476 we acquired. Using Carbachol and Atropine, to activate and inhibit the muscarinic receptors,
477 respectively, we monitored the impact on the CaT properties and found only slight
478 consequences. We found that stimulation of PC12 cells by Carbachol modulates calcium
479 release velocity and Ca^{2+} reuptake duration but did not affect the CaT of the hiPSC-CMs.
480 Moreover, inhibition of M2 muscarinic receptors in hiPSC-CMs using Atropine causes
481 increased CaT amplitude, Ca^{2+} release velocity via RyR2 and decreased Ca^{2+} reuptake
482 duration via SERCA2a. These results indicated that acetylcholine is spontaneously secreted
483 by PC12 neurites under non stimulating condition and binds to muscarinic receptors to
484 modulate Ca^{2+} kinetics affecting the SR Ca^{2+} cycling in hiPSC-CMs. Surprisingly, addition of
485 carbachol or atropine has no effects on the contractile properties compared to the results
486 obtained with Ca^{2+} experiments suggesting that spontaneous acetylcholine release is not
487 sufficient to modulate contractility. This absence of effect is possibly due to excessive
488 spontaneous secretion which would reduce the stock of neurotransmitter. During stimulation
489 of PC12 cells by carbachol, this stock of neurotransmitter may be too low and insufficient to
490 significantly impact the hiPSC-CMs contraction. This spontaneous secretion could also
491 constitutively activate the cardiac receptors which could no longer respond to a new release of
492 neurotransmitters. Another explanation could be that our neurocardiac OOC does not have
493 enough interactions between the two cell types to allow a deep modulation of the contractile

494 properties. Our data may also suggest that PC12 cell may reveal limitations to study the effect
495 of autonomic nervous system on cardiac function due to their abnormal neurotransmitter
496 secretion phenotype and the co-expression of cholinergic and catecholaminergic enzyme.

497 The use of neurons derived from hiPSC is the next step. Even if we here, as well as other
498 group [13, 37] demonstrated the feasibility of neuro-cardiac OOC from hiPSC in microfluidic
499 chips. Direct co-culture improves the maturity of peripheral neurons derived from hiPSC by
500 improving their Ca^{2+} kinetics and the expression of peripheral marker such as TH and DBH
501 [13]. The cardiac maturity was also improved by the increased expression of contractile
502 protein α -actinin and proteins involved in Ca^{2+} signaling such as RyR2 and phospholamban
503 [37]. Another group showed that culture of CMs with cortical neurons both from hiPSC in
504 microfluidic devices are able to create NCJ with limited functional effects [38]. These results
505 show that without pure autonomic neuronal population, we are limited to study NCJ and their
506 implications.

507 In this context, two groups recently published ANS differentiation protocols to obtain
508 sympathetic and/or cholinergic neurons from hiPSC. In these articles, they demonstrated that
509 autonomic neurons are able to modulate beating rate of cardiomyocytes co-cultured with
510 them. Despite these important progresses, they did not go further and observed these effects
511 on other functional properties like calcium signaling and contractile properties. Moreover, it
512 seems unclear if these neurons secrete noradrenalin or acetylcholine as desired. Further
513 experiments will be needed to obtain specific hiPSC-NRs able to impact the hiPSC-CMs
514 properties in healthy or disease-related conditions.

515 **5. Conclusions**

516 In this work, we built-up a neuro-cardiac OOC allowing to study the physiological
517 interactions between the ANS and heart during development and pathologies. We revealed the
518 presence of specialized zone between neurons and cardiomyocytes, in particular with
519 synapsin-1, a protein involved in the release of neurotransmitter-containing vesicles and
520 varicosities. Our neuro-cardiac OOC modulates the intracellular Ca^{2+} cycling of the patient-
521 derived cardiomyocytes but does not change their contractile properties. Overall, this work
522 brings evidence of the functionality of a human neurocardiac OOC to further study the
523 relationship between nervous system and heart in the dish.

524

525 **Author Contributions:** Conceptualization, A.L., B.B., E.J., J.L.P. and A.C.M.; Investigation,
526 A.A.B., S.C., C.P., B.B., V.A., Y.G., E.J. and A.C.M.; Writing, A.A.B and A.C.M.

527 **Funding:** This work was supported by grants of the “Fondation Coeur et Recherche”,
528 Association Nationale pour la Recherche Technologique (ANRT ; CIFRE N°2018/003 to
529 MicroBrain Biotech)the “Institut National pour la Santé et la Recherche Médicale”
530 (INSERM), MUSE CIBSEEA and ANR MUSAGE. Albin Bernardin received a doctoral
531 fellowship from “Le Fonds Marion Elisabeth Brancher”.

532 **Informed Consent Statement:** We obtained written informed consent from all the patients in
533 this study who agreed to have blood samples obtained for hiPSC generation. This study was
534 conducted in accordance with the Declaration of Helsinki and approved by the Institutional
535 Review Board Committee of the Montpellier Hospital (2017-A01589-44).

536 **Acknowledgments:** We thanks Dr. H el ene Delano -Ayari for her precious advices on the
537 video-edge capture analysis, and Gullen Lacin (MicroBrain BT) for chips microfabrication.

538 **Conflicts of Interest:** AB has been a full-time employee of MicroBrain BT from 2018 to
539 2021 under a CIFRE agreement (N°2018/003) to MicroBrain Biotech. BB is coinventor of the
540 patent WO2010040920A2 on neuronal diodes, and cofounder and shareholder of MicroBrain
541 Biotech S.A.S. The other authors declare no conflict of interest.

542 **References**

543

544 1. Crick SJ, A. R., Ho SY, Sheppard, MN. "Localisation and quantitation of autonomic
545 innervation in the porcine heart ii: Endocardium, myocardium and epicardium." *Journal of*
546 *Anatomy* (1999): 10.1046/j.1469-7580.1999.19530359.x.

547 2. Rajendran, P. S., R. C. Challis, C. C. Fowlkes, P. Hanna, J. D. Tompkins, M. C.
548 Jordan, S. Hiyari, B. A. Gabris-Weber, A. Greenbaum, K. Y. Chan, *et al.* "Identification of
549 peripheral neural circuits that regulate heart rate using optogenetic and viral vector strategies."
550 *Nat Commun* 10 (2019): 1944. 10.1038/s41467-019-09770-1.
551 <https://www.ncbi.nlm.nih.gov/pubmed/31028266>.

552 3. Ieda, M., H. Kanazawa, K. Kimura, F. Hattori, Y. Ieda, M. Taniguchi, J. Lee, K.
553 Matsumura, Y. Tomita, S. Miyoshi, *et al.* "Sema3a maintains normal heart rhythm through
554 sympathetic innervation patterning." *Nature medicine* (2007): 10.1038/nm1570.

555 4. Kimura, K., M. Ieda and K. Fukuda. "Development, maturation, and
556 transdifferentiation of cardiac sympathetic nerves." *Circ Res* 110 (2012): 325-36.
557 10.1161/CIRCRESAHA.111.257253. <https://www.ncbi.nlm.nih.gov/pubmed/22267838>.

558 5. Dowell, R. T. "Postnatal development of rat heart during 6-hydroxydopamine or
559 propranolol treatment." *Proc. Soc. Exp. Biol. Med.* (1985):

560 6. Kreipke, R. E. and S. J. Birren. "Innervating sympathetic neurons regulate heart size
561 and the timing of cardiomyocyte cell cycle withdrawal." *J Physiol.* (2015):
562 10.1113/JP270917.

563 7. Shcherbakova, O. G., C. M. Hurt, Y. Xiang, M. L. Dell'Acqua, Q. Zhang, R. W. Tsien
564 and B. K. Kobilka. "Organization of β -adrenoceptor signaling compartments by sympathetic
565 innervation of cardiac myocytes." *The Journal of Cell Biology* (2007):
566 10.1083/jcb.200604167.

567 8. Zaglia, T., G. Milan, M. Franzoso, E. Bertaglia, N. Pianca, E. Piasentini, V. A.
568 Voltarelli, D. Chiavegato, P. C. Brum, D. J. Glass, *et al.* "Cardiac sympathetic neurons
569 provide trophic signal to the heart via beta2-adrenoceptor-dependent regulation of
570 proteolysis." *Cardiovasc Res* 97 (2013): 240-50. 10.1093/cvr/cvs320.
571 <https://www.ncbi.nlm.nih.gov/pubmed/23090606>.

- 572 9. Taskiran Mustafa, F.-H. T., Rasmussen Verner , Larsson B W Henrik, Hilsted Jannik
573 "Decreased myocardial perfusion reserve in diabetic autonomic neuropathy." *Diabetes*
574 (2002): 10.2337/diabetes.51.11.3306.
- 575 10. Mann, D. L. and M. R. Bristow. "Mechanisms and models in heart failure: The
576 biomechanical model and beyond." *Circulation* 111 (2005): 2837-49.
577 10.1161/CIRCULATIONAHA.104.500546.
578 <https://www.ncbi.nlm.nih.gov/pubmed/15927992>.
- 579 11. Hong, J., R. J. Adam, L. Gao, T. Hahka, Z. Xia, D. Wang, T. A. Nicholas, I. H.
580 Zucker, S. J. Lisco and H. Wang. "Macrophage activation in stellate ganglia contributes to
581 lung injury-induced arrhythmogenesis in male rats." *Acta physiologica* (2021):
582 10.1111/apha.13657.
- 583 12. Gardner, M. J. K., S.; Johnstone, D.E.; Shukla, R.C.; Horacek, B.M.; Forbes, C.;
584 Armour J.A. . "The effects of unilateral stellate ganglion blockade on human cardiac function
585 during rest and exercise effects of unilateral stellate ganglion blocka." (1993): 10.1111/j.1540-
586 8167.1993.tb01207.x.
- 587 13. Oh, Y., G.-S. Cho, Z. Li, I. Hong, R. Zhu, M.-J. Kim, Yong J. Kim, E. Tampakakis, L.
588 Tung, R. Haganir, *et al.* "Functional coupling with cardiac muscle promotes maturation of
589 hpsc-derived sympathetic neurons." *Cell Stem Cell* 19 (2016): 95-106.
590 10.1016/j.stem.2016.05.002.
- 591 14. Prando, V., F. Da Broi, M. Franzoso, A. P. Plazzo, N. Pianca, M. Francolini, C. Basso,
592 M. W. Kay, T. Zaglia and M. Mangillo. "Dynamics of neuroeffector coupling at cardiac
593 sympathetic synapses: Dynamics of neurocardiac communication." *The Journal of Physiology*
594 (2018): 10.1113/JP275693.
- 595 15. Duc, P., M. Vignes, G. Hugon, A. Sebban, G. Carnac, E. Malyshev, B. Charlot and F.
596 Rage. "Human neuromuscular junction on micro-structured microfluidic devices implemented
597 with a custom micro electrode array (mea)." *Lab on a Chip* 21 (2021): 4223-36.
598 10.1039/D1LC00497B. <http://dx.doi.org/10.1039/D1LC00497B>.
- 599 16. Chiew Geraldine Giap Ying, W. N., Sultania Samiksha, Lim Sierin, Luo Kathy Qian.
600 "Bioengineered three-dimensional co-culture of cancer cells and endothelial cells: A model
601 system for dual analysis of tumor growth and angiogenesis: Analysis of tumor and vessel
602 growth in a 3d co-culture." *Biotechnology and bioengineering* (2017): 10.1002/bit.26297.

- 603 17. Arrigoni, C., S. Bersini, M. Gilardi and M. Moretti. "In vitro co-culture models of
604 breast cancer metastatic progression towards bone." *Int J Mol Sci* 17 (2016):
605 10.3390/ijms17091405. <https://www.ncbi.nlm.nih.gov/pubmed/27571063>.
- 606 18. Takeuchi, A., S. Nakafutami, H. Tani, M. Mori, Y. Takayama, H. Moriguchi, K.
607 Kotani, K. Miwa, J. Lee, M. Noshiro, *et al.* "Device for co-culture of sympathetic neurons and
608 cardiomyocytes using microfabrication." *Lab on a Chip* (2011): 10.1039/c0lc00327a.
- 609 19. Takeuchi, A., K. Shimba, M. Mori, Y. Takayama, H. Moriguchi, K. Kotani, J. Lee, M.
610 Noshiro and Y. Jimbo. "Sympathetic neurons modulate the beat rate of pluripotent cell-
611 derived cardiomyocytes in vitro." *Integrative Biology* (2012): 10.1039/c2ib20060k.
- 612 20. Acimovic, I., A. Vilotic, M. Pesl, A. Lacampagne, P. Dvorak, V. Rotrekl and A. C.
613 Meli. "Human pluripotent stem cell-derived cardiomyocytes as research and therapeutic
614 tools." *BioMed research international* 2014 (2014): 512831. 10.1155/2014/512831.
615 <http://www.ncbi.nlm.nih.gov/pubmed/24800237>.
- 616 21. Moreau, A., J. B. Reisqs, H. Delanoe-Ayari, M. Pierre, A. Janin, A. Deliniere, F.
617 Bessiere, A. C. Meli, A. Charrabi, E. Lafont, *et al.* "Deciphering dsc2 arrhythmogenic
618 cardiomyopathy electrical instability: From ion channels to ecg and tailored drug therapy."
619 *Clin Transl Med* 11 (2021): e319. 10.1002/ctm2.319.
620 <https://www.ncbi.nlm.nih.gov/pubmed/33784018>.
- 621 22. Sleiman, Y., M. Souidi, R. Kumar, E. Yang, F. Jaffre, T. Zhou, A. Bernardin, S.
622 Reiken, O. Cazorla, A. V. Kajava, *et al.* "Modeling polymorphic ventricular tachycardia at
623 rest using patient-specific induced pluripotent stem cell-derived cardiomyocytes."
624 *EBioMedicine* 60 (2020): 103024. 10.1016/j.ebiom.2020.103024.
625 <https://www.ncbi.nlm.nih.gov/pubmed/32980690>.
- 626 23. Zhang, J., M. Klos, G. F. Wilson, A. M. Herman, X. Lian, K. K. Raval, M. R. Barron,
627 L. Hou, A. G. Soerens, J. Yu, *et al.* "Extracellular matrix promotes highly efficient cardiac
628 differentiation of human pluripotent stem cells novelty and significance: The matrix sandwich
629 method." *Circulation Research* (2012): 10.1161/CIRCRESAHA.112.273144.
- 630 24. Tohyama, S., F. Hattori, M. Sano, T. Hishiki, Y. Nagahata, T. Matsuura, H.
631 Hashimoto, T. Suzuki, H. Yamashita, Y. Satoh, *et al.* "Distinct metabolic flow enables large-
632 scale purification of mouse and human pluripotent stem cell-derived cardiomyocytes." *Cell*
633 *Stem Cell* 12 (2013): 127-37. 10.1016/j.stem.2012.09.013.
634 <https://www.ncbi.nlm.nih.gov/pubmed/23168164>.

- 635 25. Winbo, A., S. Ramanan, E. Eugster, S. Jovinge, J. R. Skinner and J. M. Montgomery.
636 "Functional coculture of sympathetic neurons and cardiomyocytes derived from human
637 induced pluripotent stem cells." *American Journal of Physiology. Heart and Circulatory*
638 *Physiology* (2020): 10.1152/ajpheart.00546.2020.
- 639 26. Liu, R. H., G. Foster, E. J. Cone and S. D. Kumar. "Selecting an appropriate isotopic
640 internal standard for gas chromatography/mass spectrometry analysis of drugs of abuse--
641 pentobarbital example." *Journal of Forensic Sciences* (1995):
- 642 27. Fauconnier, J., A. C. Meli, J. Thireau, S. Roberge, J. Shan, Y. Sassi, S. R. Reiken, J.
643 M. Rauzier, A. Marchand, D. Chauvier, *et al.* "Ryanodine receptor leak mediated by caspase-
644 8 activation leads to left ventricular injury after myocardial ischemia-reperfusion." *Proc Natl*
645 *Acad Sci U S A* 108 (2011): 13258-63. 10.1073/pnas.1100286108.
646 <https://www.ncbi.nlm.nih.gov/pubmed/21788490>.
- 647 28. Lacampagne, A., X. Liu, S. Reiken, R. Bussiere, A. C. Meli, I. Lauritzen, A. F. Teich,
648 R. Zalk, N. Saint, O. Arancio, *et al.* "Post-translational remodeling of ryanodine receptor
649 induces calcium leak leading to alzheimer's disease-like pathologies and cognitive deficits."
650 *Acta Neuropathol* 134 (2017): 749-67. 10.1007/s00401-017-1733-7.
651 <https://www.ncbi.nlm.nih.gov/pubmed/28631094>.
- 652 29. Jelinkova, S., A. Vilotic, J. Pribyl, F. Aimond, A. Salykin, I. Acimovic, M. Pesl, G.
653 Caluori, S. Klimovic, T. Urban, *et al.* "Dmd pluripotent stem cell derived cardiac cells
654 recapitulate in vitro human cardiac pathophysiology." *Front Bioeng Biotechnol* 8 (2020): 535.
655 10.3389/fbioe.2020.00535. <https://www.ncbi.nlm.nih.gov/pubmed/32656189>.
- 656 30. Souidi, M., Y. Sleiman, I. Acimovic, J. Pribyl, A. Charrabi, V. Baecker, V.
657 Scheuermann, M. Pesl, S. Jelinkova, P. Skladal, *et al.* "Oxygen is an ambivalent factor for the
658 differentiation of human pluripotent stem cells in cardiac 2d monolayer and 3d cardiac
659 spheroids." *Int J Mol Sci* 22 (2021): 10.3390/ijms22020662.
660 <https://www.ncbi.nlm.nih.gov/pubmed/33440843>.
- 661 31. Taylor, A. M., S. W. Blurton-Jones M Fau - Rhee, D. H. Rhee Sw Fau - Cribbs, C. W.
662 Cribbs Dh Fau - Cotman, N. L. Cotman Cw Fau - Jeon and N. L. Jeon. "A microfluidic
663 culture platform for cns axonal injury, regeneration and transport." (2005):
- 664 32. Taylor, A. M., C. H. Rhee Sw Fau - Tu, D. H. Tu Ch Fau - Cribbs, C. W. Cribbs Dh
665 Fau - Cotman, N. L. Cotman Cw Fau - Jeon and N. L. Jeon. "Microfluidic multicompartiment
666 device for neuroscience research." (2003):

- 667 33. Habibey, R., J. E. Rojo Arias, J. Striebel and V. A.-O. Busskamp. "Microfluidics for
668 neuronal cell and circuit engineering." (2022):
- 669 34. Peyrin, J., B. Deliglise, L. Saias, M. Vignes, P. Gougis, S. Magnifico, S. Betuing, M.
670 Pietri, J. Caboche, P. Vanhoutte, *et al.* "Axon diodes for the reconstruction of oriented
671 neuronal networks in microfluidic chambers." *Lab on a Chip* (2011): 10.1039/c1lc20014c.
- 672 35. Kruepunga, N., J. Hikspoors, C. J. M. Hulsman, G. M. C. Mommen, S. E. Kohler and
673 W. H. Lamers. "Development of the sympathetic trunks in human embryos." *J Anat* 239
674 (2021): 32-45. 10.1111/joa.13415. <https://www.ncbi.nlm.nih.gov/pubmed/33641166>.
- 675 36. Hilfiker, S. P., V.A.; Czernik A.J.; Kao, H.T.; Augustine G.J.; Greengard P.
676 "Synapsins as regulators of neurotransmitter release." *Philos Trans R Soc Lond B Biol Sci*
677 (1999): 10.1098/rstb.1999.0378.
- 678 37. Kowalski, W. J., I. H. Garcia-Pak, W. Li, H. Uosaki, E. Tampakakis, J. Zou, Y. Lin,
679 K. Patterson, C. Kwon and Y. Mukoyama. "Sympathetic neurons regulate cardiomyocyte
680 maturation in culture." *Frontiers in Cell and Developmental Biology* (2022):
681 10.3389/fcell.2022.850645.
- 682 38. Hakli, M., S. Jantti, T. Joki, L. Sukki, K. Tornberg, K. Aalto-Setälä, P. Kallio, M.
683 Pekkanen-Mattila and S. Narkilahti. "Human neurons form axon-mediated functional
684 connections with human cardiomyocytes in compartmentalized microfluidic chip." *Int J Mol*
685 *Sci* 23 (2022): 10.3390/ijms23063148. <https://www.ncbi.nlm.nih.gov/pubmed/35328569>.
- 686 39. Freeman, K., W. Tao, H. Sun, M. H. Soonpaa and M. Rubart. "In situ three-
687 dimensional reconstruction of mouse heart sympathetic innervation by two-photon excitation
688 fluorescence imaging." *J Neurosci Methods* 221 (2014): 48-61.
689 10.1016/j.jneumeth.2013.09.005. <https://www.ncbi.nlm.nih.gov/pubmed/24056230>.
- 690 40. Huh, K. H. and C. Fuhrer. "Clustering of nicotinic acetylcholine receptors: From the
691 neuromuscular junction to interneuronal synapses." *Mol Neurobiol* 25 (2002): 79-112.
692 10.1385/MN:25:1:079. <https://www.ncbi.nlm.nih.gov/pubmed/11890459>.
- 693 41. Fornasiero, E. F., A. Raimondi, F. C. Guarnieri, M. Orlando, R. Fesce, F. Benfenati
694 and F. Valtorta. "Synapsins contribute to the dynamic spatial organization of synaptic vesicles
695 in an activity-dependent manner." *J Neurosci* 32 (2012): 12214-27.
696 10.1523/JNEUROSCI.1554-12.2012. <https://www.ncbi.nlm.nih.gov/pubmed/22933803>.

697 42. Rosahl, T. W. S., D.; Missler, M.; Herz, J.; Selig, D.K.; Wolff, J.R.; Hammer, R.E.;
698 Malenka, R.C.; Südhof, T.C. . "Essential functions of synapsins i and ii in synaptic vesicle
699 regulation." *Nature* (1995): 10.1038/375488a0.

700